Cellular and Molecular Life Sciences (2018) 75:2273–2289
https://doi.org/10.1007/s00018-017-2733-4

ORIGINAL ARTICLE

Bacterial LPX motif-harboring virulence factors constitute a species-spanning family of cell-penetrating effectors

Stefanie Norkowski[1] · Britta Körner[1] · Lilo Greune[1] · Anne-Sophie Stolle[1] · Marie-Luise Lubos[1] · Philip R. Hardwidge[2] · M. Alexander Schmidt[1] · Christian Rüter[1]

Received: 7 July 2017 / Revised: 22 November 2017 / Accepted: 18 December 2017 / Published online: 28 December 2017

Abstract

Effector proteins are key virulence factors of pathogenic bacteria that target and subvert the functions of essential host defense mechanisms. Typically, these proteins are delivered into infected host cells via the type III secretion system (T3SS). Recently, however, several effector proteins have been found to enter host cells in a T3SS-independent manner thereby widening the potential range of these virulence factors. Prototypes of such bacteria-derived cell-penetrating effectors (CPEs) are the *Yersinia enterocolitica*-derived YopM as well as the *Salmonella typhimurium* effector SspH1. Here, we investigated specifically the group of bacterial LPX effector proteins comprising the *Shigella* IpaH proteins, which constitute a subtype of the leucine-rich repeat protein family and share significant homologies in sequence and structure. With particular emphasis on the *Shigella*-effector IpaH9.8, uptake into eukaryotic cell lines was shown. Recombinant IpaH9.8 (rIpaH9.8) is internalized via endocytic mechanisms and follows the endo-lysosomal pathway before escaping into the cytosol. The N-terminal alpha-helical domain of IpaH9.8 was identified as the protein transduction domain required for its CPE ability as well as for being able to deliver other proteinaceous cargo. rIpaH9.8 is functional as an ubiquitin E3 ligase and targets NEMO for poly-ubiquitination upon cell penetration. Strikingly, we could also detect other recombinant LPX effector proteins from *Shigella* and *Salmonella* intracellularly when applied to eukaryotic cells. In this study, we provide further evidence for the general concept of T3SS-independent translocation by identifying novel cell-penetrating features of these LPX effectors revealing an abundant species-spanning family of CPE.

Keywords Bacterial cell-penetrating effector proteins · E3 ubiquitin ligase · IpaH · Endocytosis · Endosomal escape · LPX effector protein family

Introduction

Microbial pathogens have evolved numerous sophisticated strategies to control and modulate host cell functions for their own benefit and survival. A key virulence feature of pathogenic Gram-negative bacteria is their ability to inject effector proteins directly into targeted host cells via the type III secretion system (T3SS). Once inside the host cell, bacterial effector proteins shape the different stages of infection and particularly manipulate inflammatory signaling pathways, thereby enabling bacteria to evade the host immune system. Hence, full virulence of many bacterial pathogens often depends on the T3SS and secreted effectors [12, 31].

However, in recent years, we and others have identified several virulence factors with the capacity to translocate autonomously into mammalian and plant eukaryotic host cells without a requirement for additional bacterial factors such as the T3SS. These examples include Tir (translocated intimin receptor) from enteropathogenic *Escherichia coli* (EPEC) [11, 34], *Yersinia enterocolitica*-derived YopM (Yersinia outer protein M) [42], TcpC (Toll/interleukin-1 receptor domain containing-protein C) from uropathogenic

Electronic supplementary material The online version of this article (https://doi.org/10.1007/s00018-017-2733-4) contains supplementary material, which is available to authorized users.

✉ Christian Rüter
rueterc@uni-muenster.de

[1] Institute of Infectiology, Center for Molecular Biology of Inflammation (ZMBE), University of Münster, Von-Esmarch-Str. 56, 48149 Münster, Germany

[2] College of Veterinary Medicine, Kansas State University, 1710 Denison Ave, 101 Trotter Hall, Manhattan, KS 66506-5600, USA

E. coli (UPEC) [58], *Salmonella enterica* serovar typhimurium-derived SspH1 (Salmonella secreted protein H1) [30], the EPEC effector protein NleC (non-LEE encoded effector C) [49], and quite recently also the plant T3SS effector protein AvrBs3 from *Xanthomonas campestris* pv. *vesicatoria* [46]. These proteins share features of cell-penetrating peptides (CPP) and can translocate across eukaryotic cell membranes either alone or in association with (non-)covalently conjugated cargo [19, 27, 43]. Accordingly, these effector proteins have been termed cell-penetrating effector proteins (CPE). The mode of uptake of CPPs is still a focus of current research but is considered to mainly rely on endocytic processes followed by an endosomal escape. Furthermore, uptake mechanisms appear to depend on the targeted cell type, on the CPP's concentration, and on the associated cargo [16, 48].

The discovery of YopM from *Yersinia enterocolitica* and SspH1 from *Salmonella enterica* serovar Typhimurium as CPEs added a new class to the heterogeneous group of CPPs [30, 42]. The prototype CPE, recombinant YopM (rYopM), enters eukaryotic cells predominantly via the initial induction of endocytic mechanisms followed by escape from endosomes. Autonomously translocated rYopM was found to be functionally active in retaining its capacity to efficiently downregulate the expression of several pro-inflammatory cytokines [42, 45]. Moreover, two host kinases RSK (ribosomal S6 kinase) and PRK (protein kinase C-related kinase) were identified as interaction partners of YopM both upon T3SS-dependent delivery during *Yersinia* infection as well as following cell-penetration of rYopM [20, 22]. Lately, also the *Salmonella* effector protein SspH1 was reported to exhibit properties of a CPE exerting anti-inflammatory effects upon T3SS-independent translocation [30]. Both YopM and SspH1 belong to the family of LPX effector proteins, a subgroup of the leucine-rich repeat (LRR) motif-containing proteins. Further representatives are the *Salmonella* proteins SspH2 (*Salmonella* secreted protein H2) and SlrP (*Salmonella* leucine-rich repeat protein), as well as IpaH (Invasion plasmid antigen H) proteins expressed by *Shigella* [33]. These LPX family members share an N-terminal α-helical domain followed by a variable number of LRRs, which mediate binding and substrate specificity. The *Salmonella*- and *Shigella*-derived LPX effector proteins encode a conserved C-terminally located E3 ubiquitin ligase domain [41]. Crystal structure analyses revealed that the catalytic domain of this subset of T3SS-effector proteins is distinct from eukaryotic E3 enzymes [40, 61], hence constituting a novel class of E3 ubiquitin ligases (NEL). In contrast, YopM does not harbor this conserved NEL domain in the C-terminus, however, surprisingly a recent study suggested that due to a conserved Cys-Leu-Asp (CLD) amino acid motif in its N terminus YopM is an E3 ubiquitin ligase, too [57]. Even though bacteria lack a ubiquitin system, many pathogens hijack the host ubiquitin machinery to subvert eukaryotic defense strategies. Recent studies have uncovered the role of some NEL-encoding effector proteins in manipulating the host immune response by disabling specific target proteins in the host cell [3]. Among the *Shigella*-derived LPX effectors, IpaH9.8 is the best characterized until now. IpaH9.8 interacts with NEMO (NF-κB essential modulator, also known as IKKγ), which is critically involved in downstream activation of the NF-κB signaling cascade. IpaH9.8 promotes NEMO polyubiquitination of NEMO, which subsequently undergoes proteasomal degradation, thereby dampening NF-κB activation [4]. In addition, during *Shigella* infection, IpaH9.8 is transported to the nucleus where it binds the human splicing factor U2AF35 (U2 auxiliary cactor 35 kDa subunit) and inhibits its activity by ubiquitination, resulting in decreased U2AF35-dependent pro-inflammatory gene expression [37, 47, 52]. Several other LPX effector proteins expressed by *Salmonella* and *Shigella* also interfere with the activation of inflammatory pathways, mostly by targeting distinct target proteins for polyubiquitination leading to subsequent proteasomal degradation [3, 5, 7, 8, 13, 25, 50, 55, 60].

Although bacterial pathogens including the species of *Yersinia*, *Salmonella*, and *Shigella* have developed distinct infection strategies mediated by delivery of effector proteins exhibiting numerous biochemical activities, the LPX family represents a highly conserved subset of T3SS-translocated virulence factors. As previous studies identified two members of the LPX family, YopM and SspH1, to constitute a novel class of CPEs, the observation of significant homologies in sequence and structure raised the hypothesis of a general concept of T3SS-independent uptake of this group of bacterial effector proteins. Here, we demonstrate that, indeed, several additional members of the LPX family such as the *Shigella*-effector IpaH9.8 reveal cell-penetrating properties. Cellular internalization occurs via endocytosis and subsequent escape from the endo-lysosomal compartment. The N-terminal α-helices of IpaH9.8 were identified to mediate T3SS-independent uptake into eukaryotic cells, acting as a protein transduction domain (PTD), which can deliver also unrelated proteins. Upon cell-penetration, recombinant IpaH9.8 (rIpaH9.8) is enzymatically functional as an E3 ubiquitin ligase and polyubiquitinates NEMO. As further effectors of the LPX subtype including SlrP as well as other IpaH proteins were identified inside eukaryotic cells, our study implies the abundance of a species-spanning group of bacterial cell-penetrating effector proteins and, moreover, provides insights into novel bacterial infection strategies.

Materials and methods

Computational analyses

The 3D structures of YopM derived from *Yersinia pestis* and of the C-terminal NEL domain of IpaH9.8 derived from *Shigella flexneri* were visualized based on the crystal structure of PDB entries 1JL5 and 3L3P, respectively [15, 47]. The 3D structures of $YopM_{1–73}$ derived from *Yersinia enterocolitica* and $IpaH9.8_{1–56}$ derived from *Shigella flexneri* were predicted using the PHYRE2 Protein Fold Recognition server and modeled using PyMOL [24]. Secondary structure predictions of the sequence of $YopM_{1–73}$ and $IpaH9.8_{1–56}$ were obtained with the PSIPRED Protein Sequence Analysis Workbench server [32]. Simulations of the α-helical N termini of YopM and IpaH9.8 interacting with the membrane were performed using the MCPep server and PyMOL [18]. The alignment of $YopM_{1–337}$ and $IpaH9.8_{1–250}$ was obtained with MUSCLE with default settings and visualized using JalView before manual modification [14, 56].

Antibodies

Anti-FLAG M2 (Sigma-Aldrich, St. Louis, MO, USA), anti-GAPDH (FL-335; Santa Cruz, Dallas, TX, USA), anti-Rab5 (C8B1; Cell Signaling Technology, Danvers, MA, USA), anti-Rab7 (D95F2; Cell Signaling Technology), anti-CD63 (H5C6; Developmental Studies Hybridoma Bank, Iowa City, IA, USA), anti-HA (6E2; Cell Signaling Technology), anti-NEMO (FL-419; Santa Cruz,), anti-Ubiquitin (P4D1; Santa Cruz,), anti-α-tubulin (Sigma-Aldrich), HRP-labeled goat anti-mouse IgG (Dianova, Hamburg, Germany), HRP-labeled goat anti-rabbit IgG (Dianova), Cy2-labeled goat anti-mouse IgG (Dianova), Cy2-labeled goat anti-rabbit IgG (Dianova), and rabbit IgG anti-mouse IgG + IgM (Dianova) antibodies were obtained commercially.

Plasmids

Plasmids for the subsequent overexpression of the recombinant proteins IpaH1.4-3xFLAG, IpaH2.5-3xFLAG, IpaH4.5-3xFLAG, IpaH7.8-3xFLAG, IpaH9.8-3xFLAG, SlrP-3xFLAG, YopM-3xFLAG, $2\alpha H_{IpaH9.8}$-GFP-3xFLAG, and NEMO were cloned based on the pET-24b(+)-3xFLAG [30] or the pET-24b(+) vector, respectively. Based on the pEGFP-C1 vector, a plasmid for exogenous overexpression of human *NEMO* in eukaryotic cell lines was cloned. All above-named plasmids were generated via a restriction-free cloning approach [10, 53]. For detailed information, see supplemental material. The plasmid for the overexpression of recombinant GFP-3xFLAG has been constructed previously [30, 42]. Plasmid for the overexpression of $IpaH9.8_{\Delta N}$ (lacking amino acids 1–56) and $IpaH9.8_{\Delta C}$ (lacking amino acids 339–500) were constructed by deleting the DNA sequence coding for the indicated amino acids by inverse PCR. The plasmid pcDNA3-HA-NEMO (plasmid #13512; Addgene, Cambridge, MA, USA) was obtained commercially.

Expression, purification, and fluorescent labeling of recombinant proteins

Escherichia coli Clear Coli® BL21 (Lucigen, Middleton, WI, USA) harboring the corresponding plasmids were cultured in lysogeny broth medium supplemented with kanamycin (50 µg/mL) at 37 °C (OD_{600} = 0.7). Expression was induced by adding 1 mM of IPTG and incubation for 4 h at 37 °C. After harvesting the bacteria by centrifugation, bacterial cells were disrupted by sonication on ice four times 30 s followed by 15 s breaks, (Branson Sonifier 250, level 4, 50% cycle; Branson, Danbury, CT, USA). Isolation and purification of 6xHis-tag fusion proteins were performed by affinity chromatography using nickel–nitrilotriacetic acid (Ni–NTA) agarose beads (Macherey–Nagel, Düren, Germany) as described previously [49]. Purified proteins were dialyzed against PBS and concentrated using Centricon centrifugal filters (Merck Millipore, Billerica, MA, USA).

Recombinant proteins were conjugated with fluorescent dyes using the Cy3 antibody labeling kit (GE Healthcare, Chicago, Il, USA), the Alexa Fluor® 488 antibody labeling kit (Thermo Fisher Scientific, Waltham, MA, USA), the FluoReporter™ FITC protein labeling kit (Thermo Fisher Scientific), or 5-(and 6-) carboxynaphthofluorescein succinimidyl ester mixed isomers (naphthofluorescein, NF) (Thermo Fisher Scientific) according to the manufacturer's instructions.

Cell culture

HeLa cells were grown in DMEM low glucose (1 g/L) (Sigma-Aldrich) supplemented with 10% fetal calf serum (FCS), 5% non-essential amino acids, and penicillin/streptomycin. HEK293T cells were grown in DMEM high glucose (4.5 g/L) medium (Sigma-Aldrich) supplemented with 10% FCS, 5% non-essential amino acids, and penicillin/streptomycin. THP-1 and RAW 264.7 cells were grown in RPMI-1640 (Sigma-Aldrich) supplemented with 10% FCS, and penicillin/streptomycin. All cell lines were maintained at 37 °C in a 5% CO_2 atmosphere. The growth medium was replaced every 2–3 days.

Confocal laser scanning microscopy (CLSM)

Cells were grown in 24-well plates until 70% confluency; adherent cell lines (HeLa, HEK293T, RAW 264.7) were

directly seeded on glass coverslips, suspension cell lines (THP-1) were attached to poly-L-lysine pre-coated coverslips prior to fixation. Fluorescently labeled proteins were added to the cells. Cells were then washed three times with PBS and, to remove any residual surface bound proteins, cells were treated with acid buffer (0.2% w/v glycine in PBS, pH 2.0) for 5 min, followed again by three washes with PBS. Subsequently, the cells were fixed using 4% w/v paraformaldehyde in PBS and permeabilized using 0.2% w/v Triton X-100. Where indicated, filamentous actin was stained with tetramethyl rhodamine (TRITC)- or fluorescein isothiocyanate isomer I (FITC)-conjugated phalloidin in a 1:500 dilution in PBS for 30 min. DNA was stained with DRAQ5 in a 1:500 dilution in PBS for 30 min. Additional cellular structures were visualized using specific primary antibodies against Rab5 (early endosomes) in a 1:100 dilution in PBS, Rab7 (late endosomes) in a 1:50 dilution in PBS, and CD63 (lysosomes) in a 1:600 dilution in PBS after blocking with 5% v/v goat serum in PBS for 1 h. For detection, appropriate Cy2-labeled secondary antibodies in a 1:100 dilution in PBS were used. Cells were washed three times with PBS after each step. The preparations were embedded in DAKO fluorescent mounting medium and analyzed with a Zeiss LSM 510 Meta confocal laser scanning microscope using appropriate filters.

Cryo-electron microscopy

HeLa cells were plated in 60 mm cell culture dishes and grown for 2 days until 70% confluency. Following incubation with 50 µg/mL of rIpaH9.8-3xFLAG for 3 h, cells were fixed using 4% (w/v) paraformaldehyde in phosphate buffer (0.1 M PBS, pH 7.4) in an equal volume of culture medium for 2 min prior to fixation using 2% (w/v) paraformaldehyde and 0.25% (v/v) glutaraldehyde in phosphate buffer for additional 4 h. Afterwards, cells were washed five times with phosphate buffer, carefully scraped into 2% (w/v) gelatine in phosphate buffer and centrifuged (600×*g*, 2 min, 22 °C). Resuspension and embedding were carried out in 1.5 mL of 12% (w/v) gelatine for 5 min at 37 °C. After centrifugation (600×*g*, 2 min, 22 °C), the pellet was solidified at 4 °C and cut into small cubes which were then immersed in 2.3 M sucrose. Storage was carried out in liquid N_2. Cutting of ultrathin sections of 50 nm was performed at − 110 °C in a cryo-chamber of a Leica UC6 ultra-cryomicrotome (Leica, Vienna, Austria). For immunogold-labeling of recombinant proteins, the ultrathin sections were incubated with anti-FLAG M2 antibodies in a 1:2 dilution as primary and with rabbit anti-mouse IgG in a 1:20 dilution as secondary antibodies. Protein A-gold (15 nm) (Cell Microscopy Center-CMC, Utrecht, The Netherlands) was used to detect bound antibodies. Samples were analyzed at 80 kV with a Fei Tecnai 12-biotwin transmission electron microscope and selected areas were photographed with a Veleta side-mounted four megapixel CCD camera.

Flow cytometry

Uptake kinetics of internalized proteins were monitored using flow cytometry (FACScan flow cytometer; BD Biosciences, San Jose, CA, USA) Cellular translocation was studied by continuous time-lapse quenched uptake assays as described previously [30, 49]. Briefly, Alexa Fluor® 488-/FITC-labeled proteins in the indicated concentrations were added to trypsinized cells for continuous incubation. Upon measurement, the extracellular fluorescence was quenched using trypan blue (final concentration 0.2%). To assess the effect of different endocytic inhibitors, HeLa cells were grown in 6-well plates until 80% confluency. After pre-incubation with inhibitors (200 µM of cytochalasin D (Sigma-Aldrich), 19 mM of amiloride (Sigma-Aldrich), 30 mM of dynasore (Enzo Life Sciences, Farmingdale, NY, USA), 3.8 mM of filipin (Sigma-Aldrich), 50 mM of methyl-β-cycodextrin (Sigma-Aldrich) (MβCD), 16.5 mM of nocodazole (Sigma-Aldrich)) for 1 h, 25 µg/mL of Alexa Fluor® 488-labeled rIpaH9.8 were added to the cells for further 3 h. Before measurement, cells were trypsinized and quenched with trypan blue as described above. For uptake assays of naphthofluorescein-labeled proteins, HeLa cells were grown in 6-well plates until 80% confluency. After incubation with proteins for the indicated time periods, cells were washed three times with PBS and treated with acid buffer (0.2% w/v glycine in PBS, pH 2.0) for 5 min to remove any residual membrane-bound proteins. Unless stated otherwise, cells were incubated at 37 °C in a 5% CO_2 atmosphere. For each sample, the fluorescence intensity (GeoMean) of 10,000 cells was measured in triplicates.

In vitro ubiquitination assays

The enzymatic function of recombinant proteins as an E3 ubiquitin ligase was assessed by in vitro ubiquitination assays. These were performed in 40 µl reaction mixtures containing reaction buffer (25 mM of Tris–HCl at pH 7.5, 50 mM of NaCl, 5 mM of ATP, 10 mM of $MgCl_2$, 0.1 mM of DTT), 0.5 µg of E1, 2 µg of E2 (UbcH5b), 2.0 µg of HA-Ubiquitin (all purchased from Boston Biochem, Cambridge, MA, USA) in the presence or absence of 4 µg of the respective protein of interest. For in vitro ubiquitination of NEMO, reactions were performed accordingly except that 2 µg NEMO were added. Mixtures were incubated at 37 °C for 1 h. The reactions were stopped by adding 4 × Laemmli buffer.

TUBEs (tandem ubiquitin binding entities) pull-down assays

HEK293T cells were transiently transfected with HA-NEMO-expressing plasmid (pcDNA3-HA-NEMO) using the Effectene transfection reagent (Roche Applied Science, Penzberg, Germany) according to the manufacturer's instructions. After 24 h, cells were incubated with recombinant proteins for 6 h in the presence of 10 µM of MG132 (Sigma-Aldrich). Afterwards, cells were washed with PBS and lysed in 500 µl of RIPA lysis buffer [25 mM of Tris–HCl at pH 8.0, 137 mM of NaCl, 0.1% (w/v) SDS, 0.5% (w/v) Na-deoxycholate, 10% (v/v) glycerol, 1% (v/v) NP-40, Complete protease inhibitor cocktail (Roche)]. Lysates were cleared by centrifugation (20,000×*g*, 30 min, 4 °C) and equilibrated amounts were applied to anti-ubiquitin-TUBE agarose beads (LifeSensors, Malvern, PA, USA) for 2 h at 4 °C [21]. TUBE pull-downs were performed according to the manufacturer's instructions. Briefly, the beads were washed three times with 1% Triton X-100 in TBS prior to the elution of bound protein using the supplied elution buffer. The sample was split into two equal parts; to one half 0.5 µg of the USP2 enzyme (ubiquitin carboxyl-terminal hydrolase 2) was added, while the other half was supplemented with the appropriate amount of buffer. Both samples were incubated for 1 h at 37 °C before the reaction was stopped by adding 4 × Laemmli buffer.

Results

Shigella-derived IpaH9.8 and the *Yersinia* effector YopM share significant sequence and structural homology

Previously, the *Yersinia enterocolitica* T3SS-effector protein YopM was the first bacterial CPE that can enter eukaryotic cells independently of the T3SS to be identified [42]. Subsequently, SspH1, a T3SS-effector protein derived from *Salmonella enterica* serovar Typhimurium, was also identified as a CPE [30]. Both YopM and SspH1 belong to the group of bacterial effector proteins of the LPX subtype. Prior to experimental analyses of further members of the LPX family, investigations into sequence and structural similarities to YopM, as the prototype CPE, were performed. Initially, we focused on the *Shigella*-derived effector IpaH9.8, which represents the most extensively studied member of the LPX family. YopM (*Yersinia enterocolitica* serotype O8, strain JB580v) and IpaH9.8 (*Shigella flexneri* serotype 5a, strain M90T) share several structural features including two antiparallel α-helices at the N terminus followed by central leucine-rich repeat (LRR) domains. These reveal LPX consensus sequence motifs and, therefore, have also been referred to as LPX domain (Fig. 1a, f). The number of LRRs can differ between LPX effectors and also for a particular effector of the same species depends on the specific strain and its serotype. As representatively depicted for YopM, the LPX domain consists of several parallel β-strands which are assembled into a curved structure, giving the entire protein a 'horseshoe-shaped' structure [15] (Fig. 1b). Generally, the LPX domain is considered to mediate protein–protein interactions [26]. In contrast to YopM, which has only a small and unstructured C terminus, IpaH9.8 harbors a C-terminally located, highly conserved α-helical enzymatic domain encoding a novel class of E3 ubiquitin ligases [47] (Fig. 1c). The α-helical N termini caught our attention as this domain was previously identified as the PTD of YopM mediating autonomous, T3SS-independent translocation of the effector into eukaryotic cells [42]. Despite only moderate sequence identity of 53%, the predicted 3D structures of $YopM_{1–73}$ and $IpaH9.8_{1–56}$ almost completely overlap (Fig. 1a, d). Furthermore, computational analysis using MCPep software allowed predictions of the respective residues within this domain that might interact with the membrane bilayer (Fig S1). Based on these predictions, the orientation of the N-terminal α-helical domains of YopM and IpaH9.8 towards the membrane was simulated (Fig. 1e). For the $YopM_{1–73}$ peptide seven, for the $IpaH9.8_{1–56}$ peptide eight residues were predicted to trigger contact to the plasma membrane, thereby possibly triggering cellular uptake. During this study, we confirmed the first 56 amino acids of IpaH9.8 to be responsible for autonomous translocation into eukaryotic cells (see also Fig. 5).

rIpaH9.8 enters eukaryotic cells in a T3SS-independent manner

First, the ability of full-length IpaH9.8, expressed and purified as a recombinant protein (in the following referred as rIpaH9.8), to penetrate eukaryotic cell membranes in a T3SS-independent manner was investigated using confocal laser scanning microscopy. To this end, human cervical carcinoma (HeLa) cells were incubated with rIpaH9.8 (50 µg/mL) labeled with fluorescein isothiocyanate (FITC). By means of z-stack projections, rIpaH9.8-FITC could be detected intracellularly, predominantly in the perinuclear region in dot-like structures suggesting a vesicular localization (Fig. 2a). Increased intracellular localization was also observed over time, but nuclear localization was not observed. Recombinant green fluorescent protein (rGFP) was used as a negative control and was not detected in intracellular compartments.

Kinetic aspects of rIpaH9.8 internalization were determined using flow cytometry to monitor the uptake and intracellular accumulation of rIpaH9.8-FITC. In this approach, extracellular fluorescence was efficiently quenched by the

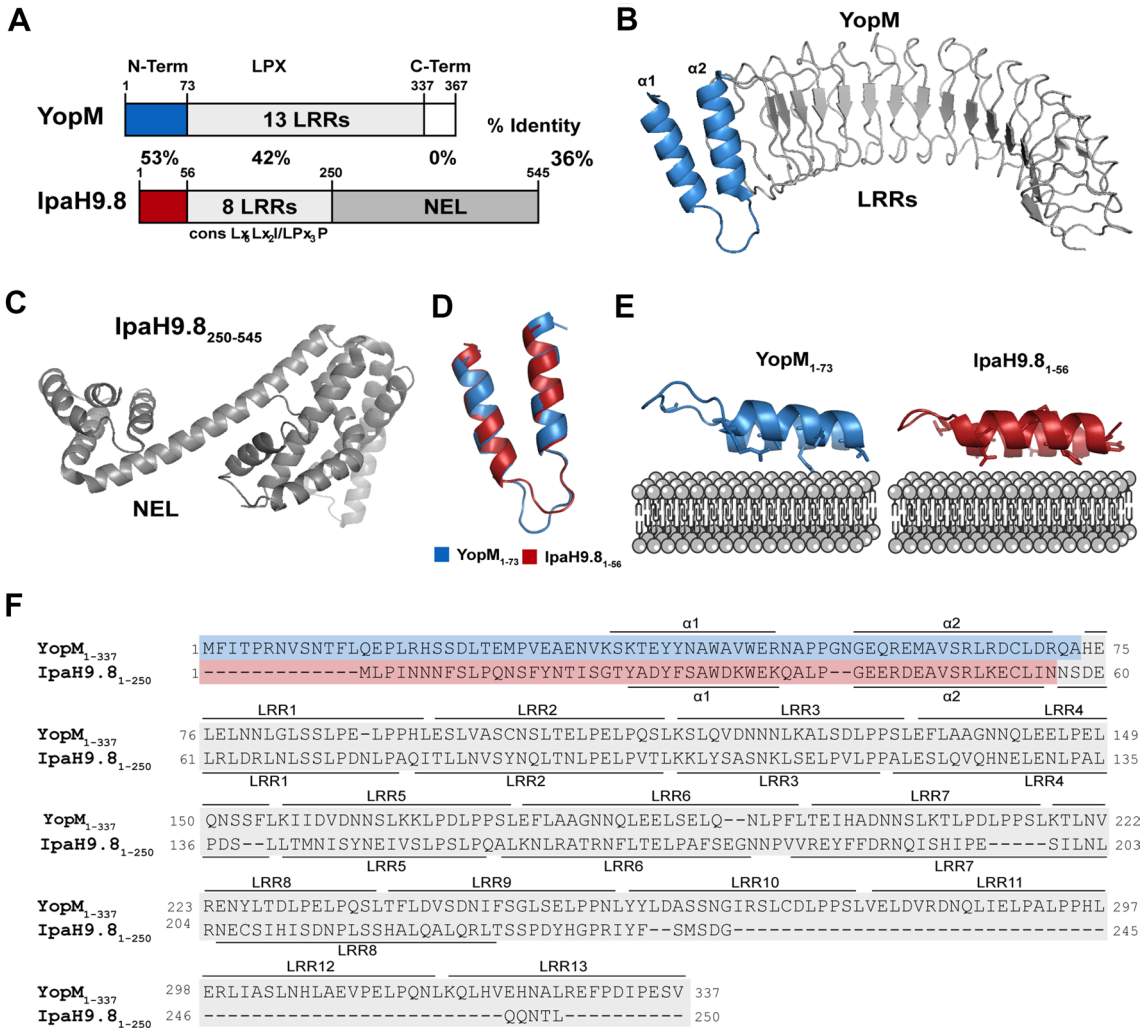

Fig. 1 Structural comparison and sequence alignment of bacterial LPX effector proteins YopM from *Yersinia enterocolitica* and IpaH9.8 from *Shigella flexneri*. **a** Schematic representation of YopM (*Yersinia enterocolitica* serotype O8, strain JB580v) and IpaH9.8 (*Shigella flexneri* serotype 5a, strain M90T). Percentage identities of the respective domains as well as of the entire proteins are indicated. *LRR* leucine-rich repeat, *NEL* novel E3 ubiquitin ligase. **b** Predicted 3D structure of YopM derived from *Yersinia pestis* (PDB: 1JL5) visualized using PyMOL. **c** Crystal structure of C-terminal novel E3 ubiquitin (NEL) domain of IpaH9.8 derived from *Shigella flexneri* (PDB: 3L3P) visualized using PyMOL. **d** Overlay of predicted 3D structures of the N-terminal α-helical domains of YopM (spanning amino acids 1–73) and IpaH9.8 (spanning amino acids 1–56) using PyMOL. **e** 3D structure simulation of the orientation of the N-terminal α-helical domains of YopM and IpaH9.8 towards the membrane bilayer. The respective residues predicted to interact with the membrane are shown as sticks. The model was generated based on predictions obtained with the MCPep server and was visualized using PyMOL. **f** Alignment of $YopM_{1–337}$ and $IpaH9.8_{1–250}$. N-terminal domains are colored in blue and red, respectively, the LPX domains are colored in gray. The localization of the α-helices in the N-terminal domains as well as the LRRs in the LPX domain is indicated with horizontal lines. The alignment was obtained with MUSCLE with default settings and visualized using JalView

addition of trypan blue allowing the measurement of only the fluorescence signals arising from intracellular FITC-labeled proteins. The mean fluorescence of HeLa cells displayed a high and linear uptake rate of rIpaH9.8, with a similar pattern as rYopM, which as a prototype CPE served as a positive control (Fig. 2b). Again, rGFP uptake was negligible. As depicted in Fig. 2c, incubation of HeLa cells with higher concentrations of rIpaH9.8-FITC (25–100 µg/mL) led to increased intracellular fluorescence in a dose-dependent manner over time. Similar conclusions were reached by studying further cell lines such as human embryonic kidney (HEK293T), human monocytic (THP-1), and murine macrophage (RAW 264.7) cells. Data obtained from flow cytometry-based analyses as well as confocal laser scanning microscopy (CLSM) analysis concordantly revealed a time-dependent cellular internalization of rIpaH9.8 into all cell lines tested (Fig S2). Differences in the mean cellular fluorescence among cell lines are attributed to the different

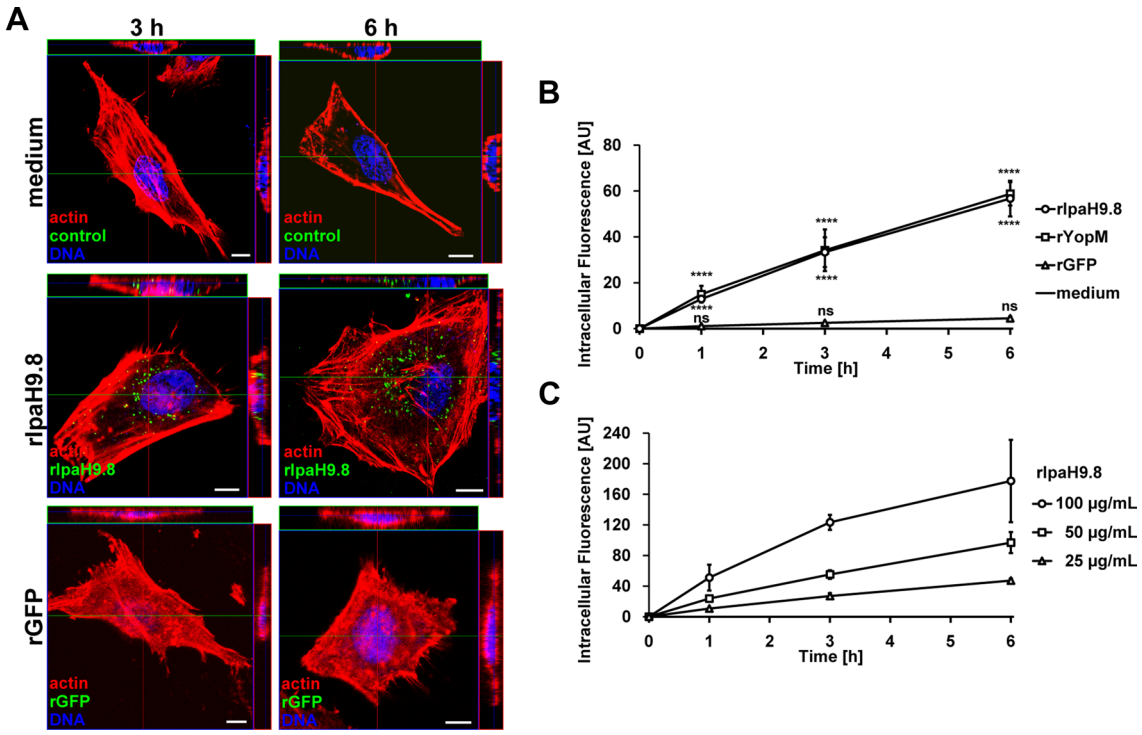

Fig. 2 T3SS-independent uptake of rIpaH9.8 into HeLa cells. **a** CLSM analysis of HeLa cells incubated with 50 µg/mL of FITC-labeled rIpaH9.8 or rGFP for 3 and 6 h, respectively. Green, FITC-labeled protein; red, actin; blue, nuclei; scale bars represent 10 µm. All images were merged and confocal z-stack projections are depicted at upper/right sides. Crosshairs indicate the position of the x–y and y–z planes. **b** Flow cytometry-based analysis of HeLa cells incubated with 25 µg/mL FITC-labeled rIpaH9.8, rYopM, or rGFP for up to 6 h. Data are means ± standard deviations from at least three independent experiments; *ns* non significant, $^{*}p < 0.05$, $^{****}p < 0.0001$ compared to medium control cells (two-way ANOVA followed by Bonferroni's multiple comparisons test). *AU* arbitrary unit. **c** Flow cytometry-based analysis of HeLa cells incubated with increasing concentrations (25–100 µg/mL) of FITC-labeled rIpaH9.8 for up to 6 h. Data are means ± standard deviations from at least three independent experiments. *AU* arbitrary unit

sizes of the different cells with HeLa cells being the largest followed by HEK293T, THP-1, and RAW 264.7 cells. Overall, these data show that rIpaH9.8 can autonomously enter eukaryotic cells.

Endocytic uptake of rIpaH9.8 is mainly mediated by macropinocytosis and lipid-raft-dependent processes

Although CPP uptake mechanisms are still not fully understood, it is commonly accepted that endocytic processes are primarily involved, whereas direct penetration of the cytoplasmic membrane was observed only in some cases [35, 51]. Comparison of uptake efficiencies at 37 and 4 °C showed that T3SS-independent translocation of rIpaH9.8 was almost completely abolished at low temperature (Fig. 3a) indicating that energy-dependent endocytic mechanisms are likely responsible. This hypothesis was followed up by co-localization analysis of internalized rIpaH9.8 with endosomal compartments. As shown in Fig. 3b, rIpaH9.8-Cy3 partially co-localized with Rab5, a marker for early endosomes, after 1 h incubation of HeLa cells. Co-localization with late endosomes (Rab7) as well as with lysosomes (CD63) was detected at later time points of 3 and 6 h, respectively (Fig. 3b).

To dissect further which endocytic pathway(s) specifically mediate(s) cellular internalization of rIpaH9.8, the effect of different inhibitors was evaluated (Fig. 3c). Pre-treatment of HeLa cells with cytochalasin D, an inhibitor of F-actin polymerization, decreased uptake of fluorescently labeled rIpaH9.8 more than 70%. A highly significant reduction of uptake of approximately 70% was also observed after inhibiting macropinocytosis using amiloride. In contrast, dynasore, an inhibitor of dynamin- and clathrin-dependent processes, only slightly altered rIpaH9.8 uptake by about 10%. The role of lipid-raft-mediated endocytosis was assessed using the inhibitors filipin and methyl-β-cyclodextrin. Both led to a significant reduction of rIpaH9.8 uptake by 50 and 75%, respectively. Microtubule dynamics, which are involved both in the formation and transport of vesicles, seem to play a role in the cellular uptake of rIpaH9.8 as nocodazole showed an inhibitory effect. Taken together, these results suggest that endocytosis, especially macropinocytosis and lipid-raft-dependent processes, mediate rIpaH9.8 internalization. To a

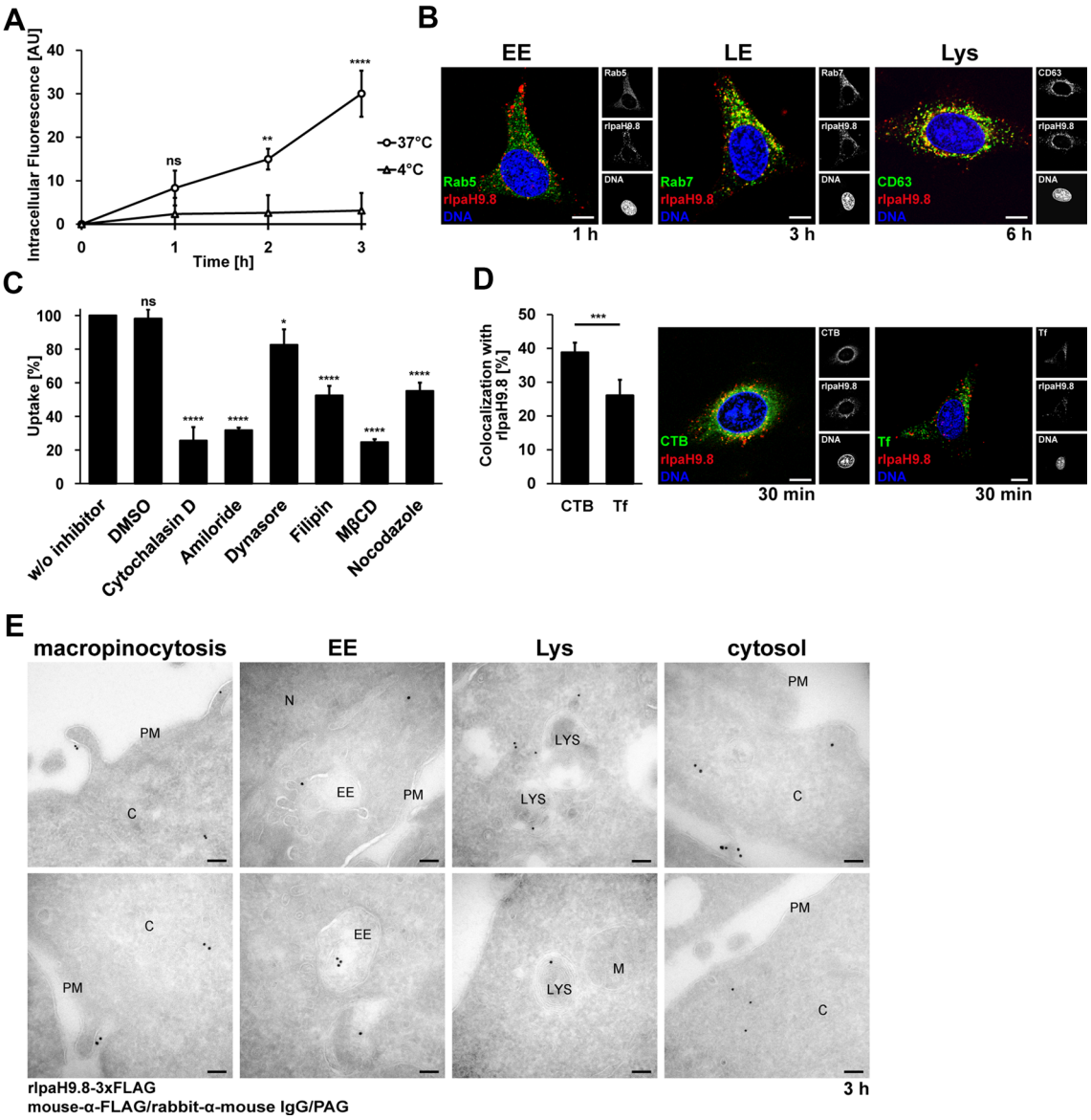

smaller extent, also clathrin-dependent endocytosis appears to be involved. This was further confirmed by co-localization analyses with fluorescently conjugated endocytic tracers. A significantly higher proportion of rIpaH9.8-Cy3 co-localized with the FITC-conjugated cholera toxin B-subunit which is internalized by caveolae-dependent mechanisms at lipid rafts, compared to Alexa Fluor®488-conjugated transferrin, a tracer for clathrin-mediated processes (Fig. 3d). This corroborates our earlier results, showing that rIpaH9.8 enters eukaryotic host cells via synergistic activities of different endocytic pathways, mainly by macropinocytosis and lipid-raft-dependent processes and less via clathrin-dependent endocytosis.

Additionally, intracellular localization was analyzed using transmission electron microscopy (Fig. 3e). FLAG-tagged rIpaH9.8 detected with Protein A-gold-conjugated-α-FLAG antibodies was found inside macropinosomes and endosomal compartments comprising early and late endosomes as well as lysosomes. In summary, these observations confirm endocytosis-dependent uptake of rIpaH9.8, which, at least partially, follows the endosomal pathways. Importantly, rIpaH9.8 was also found free in the cytosol by transmission electron microscopy. This finding is indicative of endosomal escape, which is addressed further below.

Internalized rIpaH9.8 escapes from endosomes and reaches the cytosol

Thus far, we showed an efficient cellular uptake of the LPX effector IpaH9.8 into eukaryotic cells, which is mediated by endocytic processes. However, the internalized protein needs to escape from the endo-lysosomal pathways to exert

◂**Fig. 3** Endocytic uptake of rIpaH9.8. **a** Flow cytometry-based analysis of HeLa cells incubated with 25 µg/mL Alexa Fluor®488-labeled rIpaH9.8 for up to 3 h at 37 and 4 °C, respectively. Data are means ± standard deviations from at least three independent experiments; *ns* non significant, $^{**}p < 0.01$, $^{****}p < 0.0001$ comparison of cells incubated at 37 and 4 °C (two-way ANOVA followed by Bonferroni's multiple comparisons test). *AU* arbitrary unit. **b** CLSM analysis of HeLa cells incubated with 25 µg/mL Cy3-labeled rIpaH9.8 for 1, 3 and 6 h, respectively. Merged images are shown in the left panels and single fluorescence channels are shown in the right panels. All images consist of one optical section of a z-series with a pinhole of 1 airy unit. Green, compartment-specific marker proteins for early endosomes (EE), late endosomes (LE) and lysosomes (Lys); red, Cy3-labeled rIpaH9.8; blue, nuclei; scale bars represent 10 µm. **c** Flow cytometry-based analysis of HeLa cells pre-treated with the indicated inhibitors for 1 h [200 µM cytochalasin D, 19 mM amiloride, 30 mM dynasore, 3.8 mM filipin, 50 mM methyl-β-cycodextrin (MβCD), 16.5 mM nocodazole] and subsequently incubated with 25 µg/mL Alexa Fluor®488-labeled rIpaH9.8 for 3 h. Data are means ± standard deviations from at least three independent experiments; ns, non significant, $^{*}p < 0.05$, $^{****}p < 0.0001$ compared to rIpaH9.8-incubated cells without inhibitor (one-way ANOVA followed by Bonferroni's multiple comparisons test). **d** Quantification of co-localization of rIpaH9.8-Cy3 with FITC-conjugated cholera toxin B-subunit (CTB-FITC) and Alexa Fluor®488-conjugated transferrin (Tf-Alexa Fluor®488), respectively, in HeLa cells co-incubated with either 20 µg/mL CTB-FITC or 20 µg/mL Tf-Alexa Fluor®488 and with 25 µg/mL Cy3-labeled rIpaH9.8 for 30 min. The percentages of co-localization of CTB-FITC/Tf-Alexa Fluor®488 with Cy3-labeled rIpaH9.8 were calculated using BioImageXD software. Data are means ± standard deviations after evaluating co-localization from six microscopic images; significance was calculated using the Student *t* test, $^{***}p < 0.001$ (left panel). Exemplary CLSM analysis of HeLa cells co-incubated with rIpaH9.8-Cy3 and CTB-FITC/Tf-Alexa Fluor®488. Merged images are shown in the left panels and single fluorescence channels are shown in the right panels. All images consist of one optical section of a z-series with a pinhole of 1 airy unit. Green, indicated fluorescently-labeled endocytic tracer; red, Cy3-labeled rIpaH9.8; blue, DNA; scale bars represent 10 µm (right panel). **e** Electron microscopy of cryosections of HeLa cells incubated with 50 µg/mL FLAG-tagged rIpaH9.8 for 3 h. Sections were stained with mouse-α-FLAG antibody, rabbit-α-mouse IgG antibody and Protein A Gold (PAG) (15 nm). *PM* plasma membrane, *C* cytosol, *EE* early endosome, *N* nucleus, *Lys* lysosome, *M* mitochondrion; scale bars represent 100 nm

its function in the host cell instead of undergoing lysosomal degradation.

Immunogold electron microscopy had demonstrated that after uptake rIpaH9.8 was partially located in the cytosol (Fig. 3e). As this clearly suggested the endosomal escape of internalized rIpaH9.8, this was investigated in further detail. To this end, we employed the pH-sensitive fluorescent probe naphthofluorescein (NF) used to monitor the endosomal escape and cytosolic entry of CPPs and CPEs [39, 49]. NF is well suited to monitor processes of endosomal escape as its fluorescence is quenched inside the acidic endo-lysosomal compartment, whereas in a neutral environment, such as the cytosol, it emits a fluorescent signal. This allows to easily monitor the endosomal escape of internalized NF-labeled proteins (Fig. 4a). In contrast, the previously described flow cytometry-based assay using FITC-labeled proteins solely measures total intracellular localization but does not distinguish between cytosolic or any other localization inside the cell. As depicted in Fig. 4b, incubation of HeLa cells with NF-labeled rIpaH9.8 (25 µg/mL) resulted in an increased intracellular fluorescence as measured using flow cytometry. As endosomal escape had already been confirmed for the CPE YopM, NF-labeled rYopM was included in our experiments as a positive control [45]. As expected, the addition of rYopM-NF (25 µg/mL) to HeLa cells resulted in increasing intracellular fluorescence over time, with values comparable to those measured for rIpaH9.8-NF. Bovine serum albumin (BSA) is known to follow the endo-lysosomal pathways without entering the cytosol and, thus, was used as a negative control [23]. Consequently, only background fluorescence was measurable when cells were incubated with NF-labeled BSA (25 µg/mL).

Experiments that included chloroquine, a compound that leads to endosomal swelling and rupture, and therefore, can be used to release internalized material from endosomes, indeed confirmed that BSA resides inside endosomal compartments. As shown in Fig. 4c, the addition of 150 µM chloroquine led to only moderate cytosolic delivery of BSA, whereas upon addition of 300 µM chloroquine an increase of almost 2.5-fold was observed. In contrast, for rIpaH9.8-NF, the increase in fluorescence upon addition of high concentrations of chloroquine was only minimal indicating that most of the rIpaH9.8-NF protein had already escaped from the endo-lysosomal compartment. Taken together, these results clearly demonstrate that rIpaH9.8 is delivered from endosomes into the cytosol after endocytosis-dependent cellular internalization.

The N-terminal α-helical domain of IpaH9.8 mediates cellular uptake and can deliver GFP as cargo

Cellular uptake of CPEs relies on PTDs, which can act as CPPs and thereby facilitate the delivery of further cargo molecules. To identify the domain(s) of IpaH9.8 responsible for cell-penetration, protein truncations were constructed and their T3SS-independent translocation was analyzed (Fig. 5a). The recombinant IpaH9.8$_{\Delta C}$ protein which lacks amino acids 339–500 in the C-terminally encoded NEL domain entered eukaryotic HeLa cells almost to the same extent as full-length rIpaH9.8 (Fig. 5b). However, deletion of the N-terminal α-helical domain comprising the amino acids 1–56 resulted in drastically reduced uptake rates indicating that this domain plays an important role in mediating cellular uptake of rIpaH9.8. To exclude that protein degradation during the extended incubation times (up to 8 h incubation at 37 °C) might be responsible for the observed reduced uptake, protein stability of rIpaH9.8, rIpaH9.8$_{\Delta C}$,

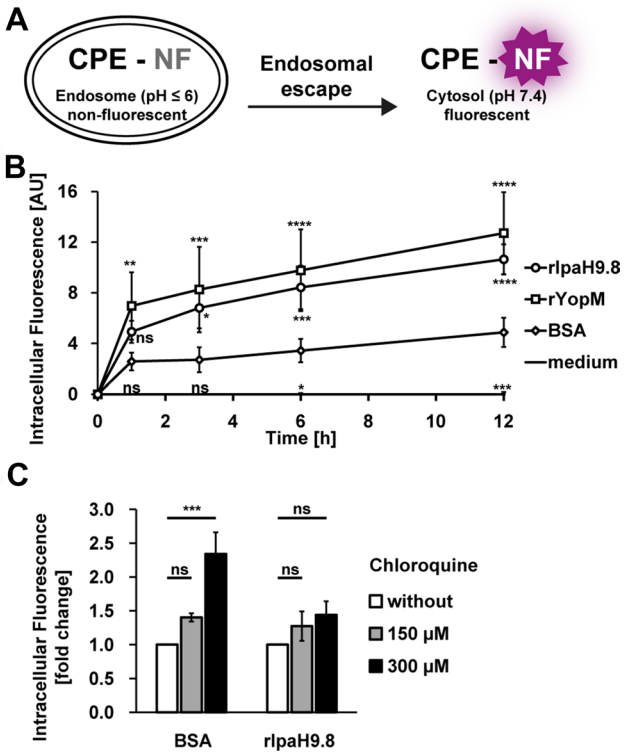

Fig. 4 Endosomal escape of internalized rIpaH9.8. **a** Schematic representation of an assay to monitor the endosomal escape of cell-penetrating effector proteins (CPE) labeled with the pH-sensitive fluorophore naphthofluorescein (NF). NF only emits fluorescence in pH neutral cytosol. **b** Flow cytometry-based analysis of HeLa cells incubated with 25 µg/mL NF-labeled rIpaH9.8, rYopM or BSA for up to 12 h. Data are means ± standard deviations from at least three independent experiments; *ns* non significant, $*p < 0.05$, $**p < 0.01$, $***p < 0.001$, $****p < 0.0001$ compared to BSA-NF-incubated cells (two-way ANOVA followed by Bonferroni's multiple comparisons test). *AU* arbitrary unit. **c** Flow cytometry-based analysis of artificially induced endosomal escape of BSA and rIpaH9.8 in HeLa cells co-incubated with 25 µg/mL NF-labeled rIpaH9.8 or BSA and increasing concentrations (150/300 µM) of chloroquine for up to 12 h. Data are means ± standard deviations from at least three independent experiments; ns, non significant, $***p < 0.001$ compared to respective control cells incubated without chloroquine (one-way ANOVA followed by Bonferroni's multiple comparisons test). *AU* arbitrary unit

and rIpaH9.8$_{\Delta N}$ under these conditions was confirmed using immunoblotting (Fig S3). Interestingly, the N-terminal two α-helices of YopM were found previously to be necessary and sufficient for uptake into eukaryotic host cells [42] and, moreover, capable of delivering cargo into target cells [19]. As illustrated in Fig. 1a, c, the N-terminal domains of YopM and IpaH9.8 display partial sequence and extended structural similarities in forming an α-helix-loop-α-helix N-terminal domain, which might be indicative of a common PTD of these two effector proteins.

Next, the ability of the N-terminal 56 amino acids of IpaH9.8 to mediate the delivery of cargo proteins was investigated. To this end, a construct consisting of the N-terminal two α-helices of IpaH9.8 fused to the N terminus of GFP was generated (Fig. 5c) and cellular uptake was assessed using flow cytometry. GFP was chosen as a model cargo protein as it is unable to enter eukaryotic host cells on its own and displays a rather rigid structure. Indeed, uptake rates of the 2αH$_{IpaH9.8}$-GFP fusion protein were almost as high as those of full-length rIpaH9.8 and even slightly higher than those of the 2αH$_{YopM}$-GFP fusion protein, which was used as a positive control. In contrast, HeLa cells did not internalize unconjugated rGFP (Fig. 5d). These findings were confirmed by performing CLSM analyses (Fig. 5e). HeLa cells incubated with 2αH$_{IpaH9.8}$-GFP (50 µg/mL) displayed intracellular fluorescence, which was evenly distributed all over the cytoplasm. A dose-dependency in GFP delivery mediated by the N-terminal α-helical domain of IpaH9.8 was also observed (Fig. 5f). Altogether, the IpaH9.8-derived N-terminal α-helical domain acts as the PTD of this effector, also enabling the delivery of cargo proteins such as GFP into eukaryotic cells.

rIpaH9.8 harbors an E3 ubiquitin ligase activity and targets NEMO for poly-ubiquitination

The *Shigella*-derived LPX effector IpaH9.8 has a C-terminally encoded novel E3 ubiquitin ligase domain that is highly conserved among the entire IpaH-SspH-SlrP family [61]. In the three-enzyme cascade of ubiquitination, E3 ligases mediate the transfer of ubiquitin to a specific target protein, thereby altering the fate of the modified substrate.

To determine whether recombinant *Shigella flexneri* (serotype 5a, strain M90T)-derived IpaH9.8 functions as an E3 ubiquitin ligase, in vitro ubiquitination assays were performed. Immunoblotting experiments showed a ladder of ubiquitin chains only in those reactions performed in the presence of either rIpaH9.8 or rIpaH9.8$_{\Delta N}$ (Fig. 6a). Control reactions lacking either E1 ubiquitin-activating or E2 ubiquitin-conjugating enzymes did not result in poly-ubiquitination. These results demonstrate that rIpaH9.8 acts as E3 ubiquitin ligase. As expected, this activity was abrogated in the rIpaH9.8$_{\Delta C}$ mutant that lacks the C-terminal domain harboring the novel E3 ligase domain. In contrast, deletion of the N-terminal α-helical domain (amino acids 1–56) did not affect the enzymatic function (Fig. 6a).

NEMO was previously identified as a target of IpaH9.8 during *Shigella* infection [4]. Interaction of rIpaH9.8 with recombinant NEMO protein (rNEMO) was confirmed using pull-down assays (Fig S4A). Ubiquitination analysis of NEMO was carried out as described above using an in vitro assay that additionally contained rNEMO. Indeed, rNEMO was poly-ubiquitinated in a rIpaH9.8-dependent manner, as indicated by an additional protein species detected by anti-NEMO antibody at a size of ≥ 48 kDa

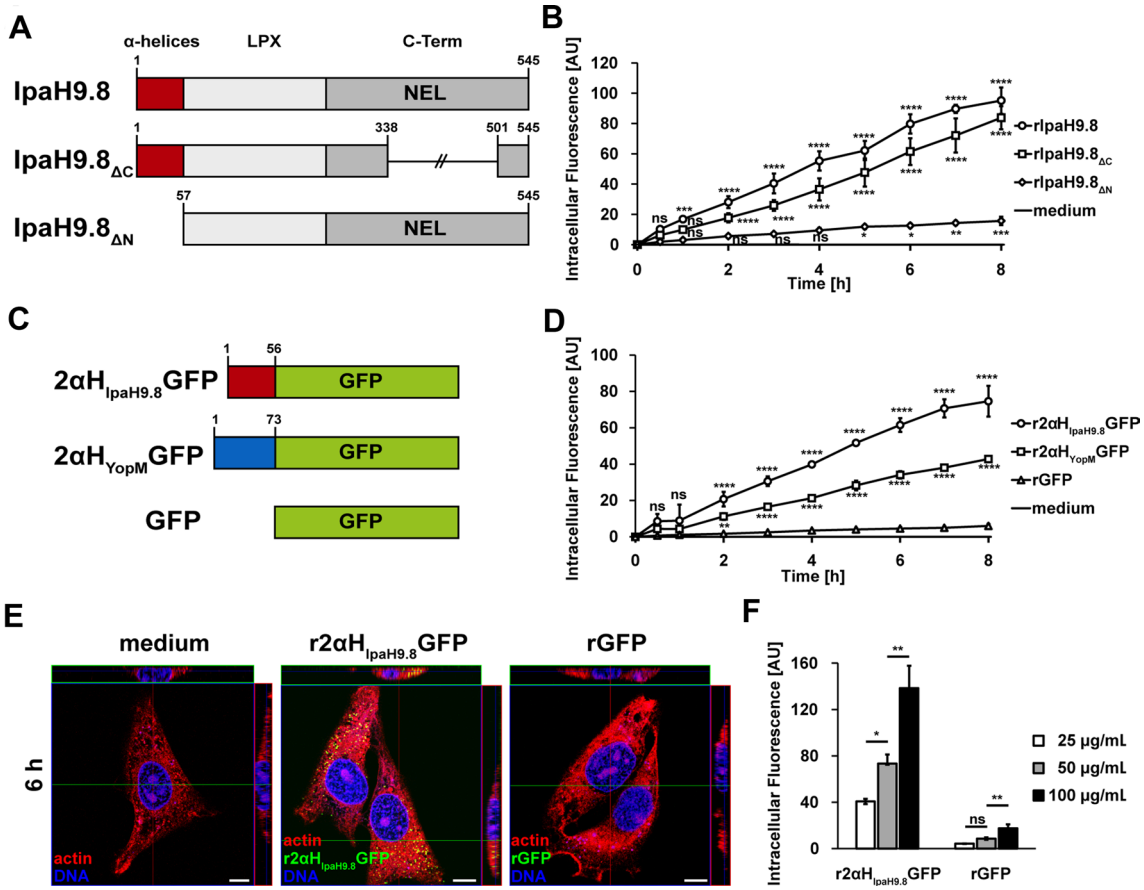

Fig. 5 The N-terminal α-helices of IpaH9.8 mediate cellular uptake and can deliver GFP as a cargo protein. **a** Schematic representation of full-length IpaH9.8 and its deletion variants IpaH9.8$_{\Delta C}$ lacking amino acids 339–500 and IpaH9.8$_{\Delta N}$ lacking amino acid 1–56. *NEL* novel E3 ubiquitin ligase. **b** Flow cytometry-based analysis of HeLa cells incubated with 0.4 µM rIpaH9.8 (= 25 µg/mL), rIpaH9.8$_{\Delta C}$ and rIpaH9.8$_{\Delta N}$ for up to 8 h. Data are means ± standard deviations from at least three independent experiments; ns, non significant, $*p < 0.05$, $**p < 0.01$, $***p < 0.001$, $****p < 0.0001$ compared to medium control cells (two-way ANOVA followed by Bonferroni's multiple comparison test). *AU* arbitrary unit. **c** Schematic representation of fusion proteins consisting of GFP fused to either the N-terminal two α-helices of IpaH9.8 (2αH$_{IpaH9.8}$GFP) or to the N-terminal 73 amino acids of YopM (2αH$_{YopM}$GFP). Non-fused GFP was used as a control. **d** Flow cytometry-based analysis of HeLa cells incubated with 25 µg/mL r2αH$_{IpaH9.8}$GFP, r2αH$_{YopM}$GFP and rGFP for up to 8 h. Data are means ± standard deviations from at least three independent experiments; *ns* non significant, $**p < 0.01$, $****p < 0.0001$ compared to rGFP-FITC-incubated cells (two-way ANOVA followed by Bonferroni's multiple comparison test). *AU* arbitrary unit. **e** CLSM analysis of HeLa cells incubated with 50 µg/mL FITC-labeled r2αH$_{IpaH9.8}$GFP and rGFP for 6 h. Green, indicated FITC-labeled protein; red, actin; blue, nuclei; scale bars represent 10 µm. All images were merged and confocal z-stack projections are depicted at upper/right sides. Crosshairs indicate the position of the x–y and y–z planes. **f** Flow cytometry-based analysis of HeLa cells incubated with increasing concentrations (25–100 µg/mL) of FITC-labeled r2αH$_{IpaH9.8}$GFP and rGFP for 6 h. Data are means ± standard deviations from at least three independent experiments; significance was calculated using one-way ANOVA followed by Bonferroni's multiple comparison test, ns, non significant, $*p < 0.05$, $**p < 0.01$. *AU* arbitrary unit

(Fig S4B). Upon cell-penetration, rIpaH9.8-mediated ubiquitination of NEMO was analyzed using TUBEs (tandem ubiquitin binding entities) pull-down assays. TUBE moieties directly coupled to agarose beads serve as high-affinity ubiquitin traps and allow to efficiently purify poly-ubiquitinated proteins from cell extracts for downstream analysis [21]. To confirm and also compare the levels of target protein poly-ubiquitination, the pull-down procedures have been combined with digestion by the broad-spectrum de-ubiquitinating enzyme USP2 prior to the ensuing analysis by Western blotting. An increased signal for the protein of interest is indicative of previous poly-ubiquitination (Fig. 6b).

To assess the levels of NEMO poly-ubiquitination, HEK293T cells over-expressing HA-tagged NEMO were incubated with increasing concentrations of rIpaH9.8 (25–100 µg/mL). We detected increased levels of HA-NEMO, as a function of rIpaH9.8 concentrations, suggesting that NEMO indeed undergoes poly-ubiquitination in a rIpaH9.8-dose-dependent manner (Fig. 6c). Only basal levels of poly-ubiquitinated HA-NEMO were observed upon incubation with the catalytically inactive rIpaH9.8$_{\Delta C}$ or

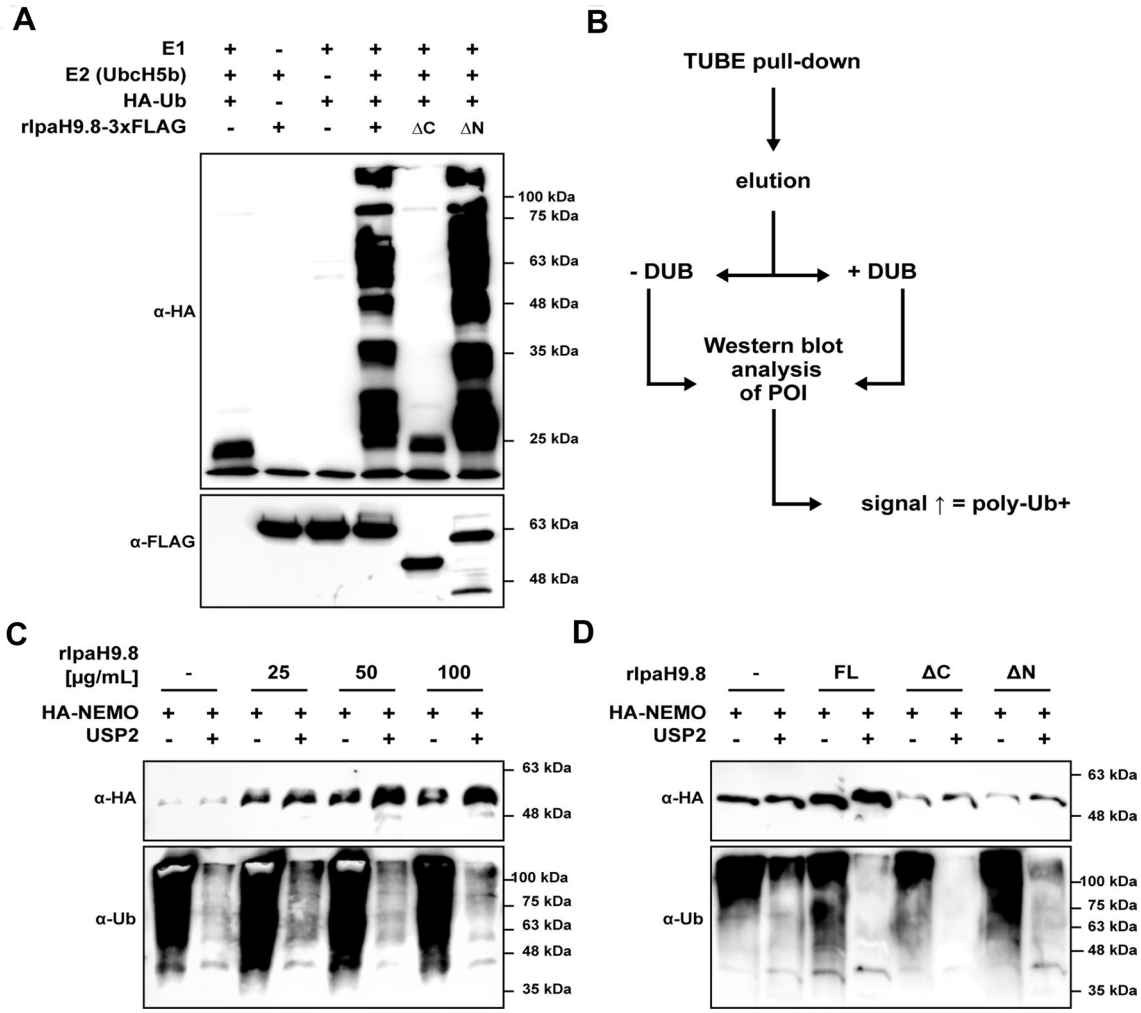

Fig. 6 rIpaH9.8 is an E3 ubiquitin ligase that poly-ubiquitinates NEMO. **a** Immunoblot detection of in vitro ubiquitination assays performed with a mixture containing E1, E2 (UbcH5b), HA-ubiquitin (HA-Ub), and either FLAG-tagged rIpaH9.8, rIpaH9.8$_{\Delta C}$, or IrpaH9.8$_{\Delta N}$. Detection of poly-ubiquitin chains using α-HA antibody; detection of indicated rIpaH9.8-3xFLAG construct using α-FLAG antibody. **b** Schematic representation of TUBEs pull-down workflow to purify and analyze poly-ubiquitinated proteins. **c** Immunoblot detection of TUBEs pull-down assay in HEK293T cells expressing HA-tagged NEMO upon 6 h incubation with rIpaH9.8-3xFLAG (25–100 µg/mL). Detection of poly-ubiquitinated HA-NEMO using α-HA antibody; detection of total level of ubiquitinated proteins (loading control) using α-ubiquitin antibody (α-Ub). Immunoblot detection of corresponding whole cell lysates is shown in Figure S4C upper panel. **d** Immunoblot detection of TUBEs pull-down assay in HEK293T cells expressing HA-NEMO upon 6 h incubation with 100 µg/mL of full-length rIpaH9.8-3xFLAG, rIpaH9.8ΔC-3xFLAG or IrpaH9.8$_{\Delta N}$-3xFLAG. Detection of poly-ubiquitinated HA-NEMO using α-HA antibody; detection of total level of ubiquitinated proteins (loading control) using α-ubiquitin antibody (α-Ub). Immunoblot detection of corresponding whole cell lysates is shown in Figure S4C lower panel

with the non-penetrating rIpaH9.8$_{\Delta N}$ protein (each 100 µg/mL) (Fig. 6d). We conclude that cell-penetrating and enzymatically functional rIpaH9.8 mediates poly-ubiquitination of its target host protein NEMO not only in vitro but also intracellularly following T3SS-independent translocation. How this affects the fate of NEMO is still unclear. Proteasomal degradation of ubiquitinated NEMO is currently a controversial issue and was not observed upon rIpaH9.8-mediated ubiquitination (data not shown) [4, 13].

T3SS-independent translocation: a common feature of LPX effector proteins

YopM and SspH1 belong to the LPX family of bacterial effector proteins, which further comprises the *Salmonella* proteins SspH2 and SlrP, as well as different *Shigella* IpaH proteins. Since effector proteins of the LPX family share significant homology in sequence and structure [33] the ability of other family members to autonomously translocate

through the plasma membrane of eukaryotic cells in a T3SS-independent manner was investigated. We recombinantly expressed and purified IpaH1.4, IpaH2.5, IpaH4.5, IpaH7.8, and SlrP and analyzed their cell-penetrating properties. Figure 7 summarizes the results of flow cytometry-based analyses of HeLa cells upon incubation with the different fluorescently labeled LPX proteins (each 25 µg/mL). In all cases, increasing intracellular fluorescence intensities were measured indicating efficient internalization (Fig. 7a–e, left panel). Confocal fluorescence microscopy of HeLa cells incubated with Cy3-labeled rIpaH1.4, rIpaH2.5, rIpaH4.5, rIpaH7.8, and rSlrP (each 25 µg/mL) revealed that all recombinant LPX effector proteins entered the cells. The proteins were found in slightly different amounts and predominantly localized in the perinuclear region both after 1 and 3 h similar to rIpaH9.8. Nuclear localization was not observed (Fig. 7a–e, right panel).

In summary, this study provides convincing experimental evidence for the functional characterization of rIpaH9.8 as an autonomously cell-entering effector protein or CPE. In addition, these findings further support the general concept of T3SS-independent translocation of bacterial effector proteins of the LPX subtype.

Discussion

In the present study, we have characterized the cell-penetrating abilities of bacterial effector proteins of the LPX subtype. Focusing on the *Shigella*-derived effector protein IpaH9.8, we observed T3SS-independent internalization via macropinocytosis and lipid raft-dependent endocytosis, followed by endosomal escape.

Although we observed striking sequence and structural homologies between IpaH9.8 and the N-terminal α-helical PTD of YopM (Fig. 1), no obvious similarities to other PTDs of known CPPs could be identified. Employing different experimental approaches, we demonstrated the ability of rIpaH9.8 to enter eukaryotic cells autonomously in a time- and dose-dependent manner (Fig. 2). This appears to be an intrinsic property as it could be observed in different eukaryotic cell lines (Fig S2). rIpaH9.8 uptake was impaired at low temperature compared to physiological 37 °C suggesting the involvement of energy-dependent uptake processes (Fig. 3a). Microscopic analyses that revealed endo-lysosomal localization of internalized rIpaH9.8 support a model for endocytic uptake. However, we cannot completely exclude an additional contribution of direct penetration as this mechanism might also be affected by the diminished fluidity of the cytoplasmic membrane at lower temperatures.

rIpaH9.8 uptake was highly reduced by blocking actin polymerization, which is involved in vesicle formation and transport. The fact that inhibiting microtubules, which are essential for intracellular trafficking, also influenced uptake dynamics suggests that rIpaH9.8 utilizes endocytic vesicle formation and subsequent intracellular trafficking to gain access into eukaryotic host cells (Fig. 3c). Nowadays, the majority of CPPs is described to follow the endocytic uptake route [48], which has also been shown previously for the cell-penetrating LPX effectors YopM and SspH1 [30, 42]. Computational predictions uncovered several amino acids in the N-terminal α-helical domain of rIpaH9.8 that might potentially interact with the plasma membrane (Fig. 1d and Fig S1). This initial contact could trigger the subsequent cellular internalization of the effector protein thereby supporting a receptor-independent endocytic mode of uptake. This is consistent with our findings that macropinocytosis and lipid-raft-dependent processes were especially important in mediating cellular internalization of rIpaH9.8 (Fig. 3c, d). Indeed, IpaH9.8's domain spanning the first 56 amino acids not only exhibits high similarity to the N-terminal part of YopM but also, in this study, was confirmed experimentally to mediate T3SS-independent translocation. Furthermore, this domain functioned as a PTD and delivered GFP into eukaryotic cells (Fig. 5). Hence, the identification of the N-terminal α-helical domain of IpaH9.8 as a novel PTD opens the possibility to deliver heterologous cargos. In this context, in combination with, e.g., homing peptides, novel combinatorial strategies for targeted therapeutic approaches might be developed. Based on these findings, IpaH9.8 meets the criteria to be considered as a CPP/CPE because of (1) its autonomous translocation into eukaryotic cells, (2) its uptake mediated by a distinct PTD and (3) its ability to transport heterologous cargo into eukaryotic cells.

Internalized rIpaH9.8 seems to, at least partially, follow the endo-lysosomal pathway. Especially at later time points, lysosomal localization was observed (Fig. 3b). Nonetheless, we can demonstrate that internalized rIpaH9.8 is able to avoid complete degradation inside lysosomes by escaping into the cytosol. Initial indications for endosomal escape were provided by electron microscopy analysis revealing internalized rIpaH9.8 to be localized partially free in the cytosol (Fig. 3e). These observations were substantiated by flow cytometry-based measurements using naphthofluorescein-labeled rIpaH9.8 (Fig. 4). The pH-sensitive dye naphthofluorescein allows to exclusively measure fluorescence arising from cytosolic proteins since it only emits fluorescence in a neutral environment such as in the cytosol. Extracellular fluorescence is quenched by an acid buffer. The slight increase in fluorescence with BSA-NF-incubated cells is most probably due to residual fluorescence arising from early endosomes which are not fully acidified. In comparison to BSA-NF distinct increases for both rIpaH9.8 and rYopM in NF-dependent fluorescence already found after short incubation time clearly point to a cytosolic localization of both proteins.

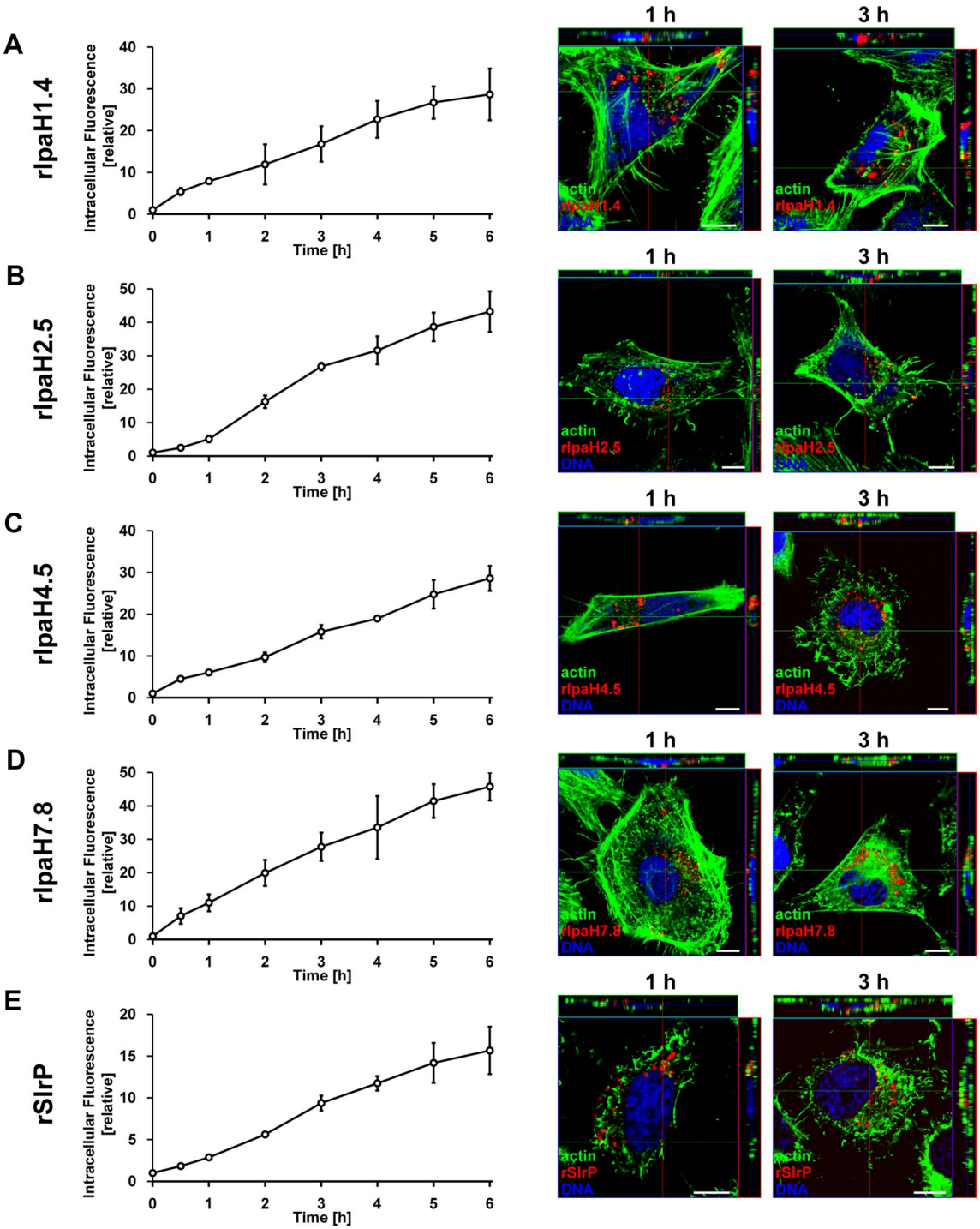

Fig. 7 Several bacterial LPX effector proteins enter HeLa cells in a T3SS-independent manner. Flow cytometry-based analysis of HeLa cells incubated with 25 µg/mL Alexa Fluor®488-labeled **a** rIpaH1.4, **b** rIpaH2.5, **c** rIpaH4.5, **d** rIpaH7.8, or **e** rSlrP for up to 6 h. Data are means ± standard deviations from three independent experiments (left panels). CLSM analysis of HeLa cells incubated with 25 µg/mL of Cy3-labeled **a** rIpaH1.4, **b** rIpaH2.5, **c** rIpaH4.5, **d** rIpaH7.8, or **e** rSlrP for 1 and 3 h, respectively. Red, Cy3-labeled rIpaH9.8; green, actin; blue, nuclei; scale bars represent 10 µm. All images were merged and confocal z-stack projections are depicted at upper/right sides. Crosshairs indicate the position of the x–y and y–z planes (right panels)

Ubiquitination of NEMO in a rIpaH9.8-dependent manner can be taken as additional evidence for the effector's ability to reach the cytosol where it functions as an E3 ubiquitin ligase (Fig. 6). This resembles the infection scenario in which NEMO was first identified as a target of IpaH9.8 [4]. This implies that intracellular activity and protein interactions of autonomously translocated and T3SS-injected IpaH9.8 are at least partially overlapping.

For now, it remains elusive how rIpaH9.8 escapes into the cytosol of HeLa cells. In general, there are different models describing endosomal escape mechanisms of internalized proteins. These models include escape from endosomes by retrograde trafficking via the Golgi network to the endoplasmic reticulum, from where proteins are released into the cytosol, penetration of endosomal membranes upon pH-induced conformational changes of internalized proteins, or the induction of transient pores into the vesicular membrane [9, 17, 54]. Measurements of potential alterations in the protein's three-dimensional structure that were obtained using the fluorophore 6,*P*-toluidinyl-naphthalene-2-sulfonate (TNS) [2] as a hydrophobicity marker showed that rIpaH9.8 indeed undergoes a pH-dependent conformational shift (Fig S5 A–B). Furthermore, the inhibition of endosomal acidification by Bafilomycin A1, an inhibitor of vacuolar H^+-ATPases, resulted in an impaired intracellular functionality of rIpaH9.8 as detected by diminished levels of poly-ubiquitinated HA-NEMO (Fig S5 C). Together, these data suggest the endosomal acidification is needed to induce conformational alterations in the rIpaH9.8 protein which then in turn facilitates endosomal escape of the cell-penetrating LPX effector protein.

Generally, the identification of cell-penetrating bacterial effector proteins opens the possibilities to study its intracellular functionality in the absence of other, potentially interfering bacterial components. Whether during *Shigella* infection-secreted ('recombinant') IpaH9.8 might play a substantial role in virulence cannot be assessed from the current data and needs to be addressed in future investigations. This is also true for the other LPX family members where in most cases it is not known whether these effector proteins might be secreted into the extracellular environment during infection. However, the increasing number of effector proteins that overcome eukaryotic membranes autonomously might point towards a biological role during bacterial infections. This notion is further supported by our identification of the LPX effector proteins, a species-spanning group of virulence factors, which not only share similarities in sequence and structure but also apparently their ability to translocate into eukaryotic cells in a T3SS-independent manner (Fig. 7). From an evolutionary point of view, autonomous translocation of effector proteins might be considered as a relic from times prior to the evolution of highly efficient bacterial secretion machineries, when cell-penetrating abilities of secreted virulence proteins might have been advantageous. The bacterial flagellum, the ancestor of the T3SS machinery, is able to secrete proteins, including bacterial effectors, under certain environmental conditions [1, 28, 59]. However, over millions of years bacteria have evolved the T3SS apparatus which allows direct cellular injection and targeting of host cell functions in a more specialized and efficient manner as compared to flagellar secretion. Directly injected effector proteins enjoy the further advantage of being protected from the immune system. Therefore, CPEs might be considered as an evolutionary artifact from antecedent bacterial infections.

On the other hand, autonomous, T3SS-independent translocation might also still be relevant and might provide an additional advantage to a sole T3SS-mediated injection of effector proteins. In contrast to T3SS-delivery, autonomous mechanisms do not require direct bacterial attachment to the host cells and, therefore, might affect also 'by-stander' cells of the specific tissue, thereby facilitating further dissemination and extended bacterial infections. In this regard, flagellar export of bacterial effector proteins could also be involved as it has been reported for different species previously [28, 59]. Moreover, it is not yet known whether T3SS-dependent secretion of LPX effector proteins can be induced exclusively by contact with intact cells or also by contact with cell fragments (e.g., exosomes) or other tissue components. After all, it was shown that secretion of effector proteins can be stimulated artificially by several inducer molecules including Congo Red [6, 29]. Interestingly, exogenously added YopM is able to partially restore the impaired virulence of a Δ*yopM* strain [36]. In a previous study, the EPEC effector protein NleC was found to display characteristics of bacterial A-B toxins, underlining the hypothesis that bacterial effector proteins have multiple ways to enter host cells [49]. Undeniably, T3SS-mediated injection constitutes the major delivery route of bacterial effectors, but, autonomously translocated CPEs might synergize with and extend this pathogenicity module.

The cell-penetrating abilities and enzymatic activities of rIpaH9.8 and other bacterial effector proteins make these proteins highly interesting in terms of therapeutic applications. Whether ubiquitination of NEMO or of other (so far unknown) targets upon autonomous translocation of rIpaH9.8 has an impact on the transcriptional profile of pro-inflammatory cytokines remains to be investigated. Here, we provide evidence that autonomously translocated rIpaH9.8 is able to target and interfere with the host ubiquitin system. Although bacteria lack a ubiquitin system of their own, quite a few have apparently developed hijacking tools for the host's ubiquitin machinery to modulate essential host cell functions for their own benefit. Hence, several studies on bacterial effector proteins that manipulate specific post-translational modification pathways such as ubiquitination aim to identify new targets for the development of effective

anti-microbial drugs. Apart from that, a better understanding of the 'microbial knowledge' might also uncover an extensive toolkit of natural modulators of many essential host processes. This change of paradigm was previously proposed as the 'drugs from bugs concept' [43, 44]. As alterations in the ubiquitin system contribute to the development of distinct diseases [38], cell-penetrating effector proteins with ubiquitin E3 ligase activities such as the LPX proteins might be of therapeutic interest. The present study provides an encouraging basis to follow this up in the future.

Acknowledgements We like to thank our colleagues of the Institute of Infectiology for fruitful discussions and their valuable contributions.

Funding This study was supported by Grants from the Deutsche Forschungsgemeinschaft (DFG, RU1884/2-1 to CR, SFB1009 TP B03 to CR and MAS), by the DFG Graduiertenkolleg GRK1409, the Cells-in-Motion Cluster of Excellence (EXC 1003-CiM), and by a Grant from the Interdisciplinary Centre for Clinical Research (IZKF, Rüt2/002/16 to CR) of the Medical Faculty of the University of Münster. The funders had no role in study design, data collection and interpretation, or the decision to submit the work for publication.

References

1. Abby SS, Rocha EP (2012) The non-flagellar type III secretion system evolved from the bacterial flagellum and diversified into host-cell adapted systems. PLoS Genet 8:e1002983. https://doi.org/10.1371/journal.pgen.1002983
2. Albani JR (2009) Fluorescence origin of 6, *P*-toluidinyl-naphthalene-2-sulfonate (TNS) bound to proteins. J Fluoresc 19:399–408. https://doi.org/10.1007/s10895-008-0426-y
3. Ashida H, Kim M, Sasakawa C (2014) Exploitation of the host ubiquitin system by human bacterial pathogens. Nat Rev Microbiol 12:399–413. https://doi.org/10.1038/nrmicro3259
4. Ashida H, Kim M, Schmidt-Supprian M, Ma A, Ogawa M, Sasakawa C (2010) A bacterial E3 ubiquitin ligase IpaH9.8 targets NEMO/IKKgamma to dampen the host NF-kappaB-mediated inflammatory response. Nat Cell Biol 12(66–73):1–9. https://doi.org/10.1038/ncb2006
5. Ashida H, Nakano H, Sasakawa C (2013) *Shigella* IpaH0722 E3 ubiquitin ligase effector targets TRAF2 to inhibit PKC-NF-kappaB activity in invaded epithelial cells. PLoS Pathog 9:e1003409. https://doi.org/10.1371/journal.ppat.1003409
6. Bahrani FK, Sansonetti PJ, Parsot C (1997) Secretion of Ipa proteins by *Shigella flexneri*: inducer molecules and kinetics of activation. Infect Immun 65:4005–4010
7. Bernal-Bayard J, Cardenal-Munoz E, Ramos-Morales F (2010) The *Salmonella* type III secretion effector, *Salmonella* leucine-rich repeat protein (SlrP), targets the human chaperone ERdj3. J Biol Chem 285:16360–16368. https://doi.org/10.1074/jbc.m110.100669
8. Bhavsar AP, Brown NF, Stoepel J, Wiermer M, Martin DD, Hsu KJ, Imami K, Ross CJ, Hayden MR, Foster LJ, Li X, Hieter P, Finlay BB (2013) The *Salmonella* type III effector SspH2 specifically exploits the NLR co-chaperone activity of SGT1 to subvert immunity. PLoS Pathog 9:e1003518. https://doi.org/10.1371/journal.ppat.1003518
9. Bonifacino JS, Rojas R (2006) Retrograde transport from endosomes to the trans-Golgi network. Nat Rev Mol Cell Biol 7:568–579
10. Chen GJ, Qiu N, Karrer C, Caspers P, Page MG (2000) Restriction site-free insertion of PCR products directionally into vectors. BioTechniq 28:498–500 **(504–505)**
11. Cirl C, Wieser A, Yadav M, Duerr S, Schubert S, Fischer H, Stappert D, Wantia N, Rodriguez N, Wagner H, Svanborg C, Miethke T (2008) Subversion of Toll-like receptor signaling by a unique family of bacterial Toll/interleukin-1 receptor domain-containing proteins. Nat Med 14:399–406. https://doi.org/10.1038/nm1734
12. Coburn B, Sekirov I, Finlay BB (2007) Type III secretion systems and disease. Clin Microbiol Rev 20:535–549
13. de Jong MF, Liu Z, Chen D, Alto NM (2016) *Shigella flexneri* suppresses NF-kappaB activation by inhibiting linear ubiquitin chain ligation. Nat Microbiol 1:16084. https://doi.org/10.1038/nmicrobiol.2016.84
14. Edgar RC (2004) MUSCLE: a multiple sequence alignment method with reduced time and space complexity. BMC Bioinf 5:113. https://doi.org/10.1186/1471-2105-5-113
15. Evdokimov AG, Anderson DE, Routzahn KM, Waugh DS (2001) Unusual molecular architecture of the *Yersinia pestis* cytotoxin YopM: a leucine-rich repeat protein with the shortest repeating unit. J Mol Biol 312:807–821. https://doi.org/10.1006/jmbi.2001.4973
16. Fischer R, Fotin-Mleczek M, Hufnagel H, Brock R (2005) Break on through to the other side-biophysics and cell biology shed light on cell-penetrating peptides. Chembiochem 6:2126–2142. https://doi.org/10.1002/cbic.200500044
17. Fischer R, Kohler K, Fotin-Mleczek M, Brock R (2004) A stepwise dissection of the intracellular fate of cationic cell-penetrating peptides. J Biol Chem 279:12625–12635. https://doi.org/10.1074/jbc.m311461200
18. Gofman Y, Haliloglu T, Ben-Tal N (2012) Monte Carlo simulations of peptide-membrane interactions with the MCPep web server. Nucleic Acids Res 40:W358–W363. https://doi.org/10.1093/nar/gks577
19. Gomarasca M, Martins TFC, Greune L, Hardwidge PR, Schmidt MA, Rüter C (2017) Bacterium-derived cell-penetrating peptides deliver gentamicin to kill intracellular pathogens. Antimicrob Agents Chemother. https://doi.org/10.1128/aac.02545-16
20. Hentschke M, Berneking L, Belmar Campos C, Buck F, Ruckdeschel K, Aepfelbacher M (2010) *Yersinia* virulence factor YopM induces sustained RSK activation by interfering with dephosphorylation. PLoS One. https://doi.org/10.1371/journal.pone.0013165
21. Hjerpe R, Aillet F, Lopitz-Otsoa F, Lang V, England P, Rodriguez MS (2009) Efficient protection and isolation of ubiquitylated proteins using tandem ubiquitin-binding entities. EMBO Rep 10:1250–1258. https://doi.org/10.1038/embor.2009.192
22. Höfling S, Scharnert J, Cromme C, Bertrand J, Pap T, Schmidt MA, Rüter C (2014) Manipulation of pro-inflammatory cytokine production by the bacterial cell-penetrating effector protein YopM is independent of its interaction with host cell kinases RSK1 and PRK2. Virulence 5:761–771. https://doi.org/10.4161/viru.29062
23. Humphries WH 4th, Payne CK (2012) Imaging lysosomal enzyme activity in live cells using self-quenched substrates. Anal Biochem 424:178–183. https://doi.org/10.1016/j.ab.2012.02.033
24. Kelley LA, Mezulis S, Yates CM, Wass MN, Sternberg MJ (2015) The Phyre2 web portal for protein modeling, prediction and analysis. Nat Protoc 10:845–858. https://doi.org/10.1038/nprot.2015.053
25. Keszei AF, Tang X, McCormick C, Zeqiraj E, Rohde JR, Tyers M, Sicheri F (2014) Structure of an SspH1-PKN1 complex reveals the basis for host substrate recognition and mechanism of activation for a bacterial E3 ubiquitin ligase. Mol Cell Biol 34:362–373. https://doi.org/10.1128/mcb.01360-13
26. Kobe B, Kajava AV (2001) The leucine-rich repeat as a protein recognition motif. Curr Opin Struct Biol 11:725–732

27. Langel Ü (2005) Handbook of cell-penetrating peptides. CRC Press, Taylor & Francis Group, Boca Raton
28. Lee SH, Galán JE (2004) *Salmonella* type III secretion-associated chaperones confer secretion-pathway specificity. Mol Microbiol 51:483–495. https://doi.org/10.1046/j.1365-2958.2003.03840.x
29. Liu X, Lu L, Liu X, Liu X, Pan C, Feng E, Wang D, Niu C, Zhu L, Wang H (2016) Proteomic analysis of *Shigella* virulence effectors secreted under different conditions. J Microbiol Biotechnol. https://doi.org/10.4014/jmb.1603.03015
30. Lubos M, Norkowski S, Stolle A, Langel Ü, Schmidt MA, Rüter C (2014) Analysis of T3SS-independent autonomous internalization of the bacterial effector protein SspH1 from *Salmonella typhimurium*. Inflamm Cell Signal 1:1–10. https://doi.org/10.14800/ics.423
31. Mattoo S, Lee YM, Dixon JE (2007) Interactions of bacterial effector proteins with host proteins. Curr Opin Immunol 19:392–401
32. McGuffin LJ, Bryson K, Jones DT (2000) The PSIPRED protein structure prediction server. Bioinformatics 16:404–405
33. Miao EA, Scherer CA, Tsolis RM, Kingsley RA, Adams LG, Baumler AJ, Miller SI (1999) *Salmonella typhimurium* leucine-rich repeat proteins are targeted to the SPI1 and SPI2 type III secretion systems. Mol Microbiol 34:850–864. https://doi.org/10.1046/j.1365-2958.1999.01651.x
34. Michgehl S, Heusipp G, Greune L, Rüter C, Schmidt MA (2006) Esp-independent functional integration of the translocated intimin receptor (Tir) of enteropathogenic *Escherichia coli* (EPEC) into host cell membranes. Cell Microbiol 8:625–633
35. Mitchell DJ, Kim DT, Steinman L, Fathman CG, Rothbard JB (2000) Polyarginine enters cells more efficiently than other polycationic homopolymers. J Pept Res 56:318–325
36. Nemeth J, Straley SC (1997) Effect of *Yersinia pestis* YopM on experimental plague. Infect Immun 65:924–930
37. Okuda J, Toyotome T, Kataoka N, Ohno M, Abe H, Shimura Y, Seyedarabi A, Pickersgill R, Sasakawa C (2005) *Shigella* effector IpaH9.8 binds to a splicing factor U2AF(35) to modulate host immune responses. Biochem Biophys Res Commun 333:531–539
38. Popovic D, Vucic D, Dikic I (2014) Ubiquitination in disease pathogenesis and treatment. Nat Med 20:1242–1253. https://doi.org/10.1038/nm.3739
39. Qian Z, Dougherty PG, Pei D (2015) Monitoring the cytosolic entry of cell-penetrating peptides using a pH-sensitive fluorophore. Chem Commun (Camb) 51:2162–2165. https://doi.org/10.1039/c4cc09441g
40. Quezada CM, Hicks SW, Galán JE, Stebbins CE (2009) A family of *Salmonella* virulence factors functions as a distinct class of autoregulated E3 ubiquitin ligases. Proc Natl Acad Sci USA 106:4864–4869. https://doi.org/10.1073/pnas.0811058106
41. Rohde JR, Breitkreutz A, Chenal A, Sansonetti PJ, Parsot C (2007) Type III secretion effectors of the IpaH family are E3 ubiquitin ligases. Cell Host Microbe 1:77–83
42. Rüter C, Buss C, Scharnert J, Heusipp G, Schmidt MA (2010) A newly identified bacterial cell-penetrating peptide that reduces the transcription of pro-inflammatory cytokines. J Cell Sci 123:2190–2198. https://doi.org/10.1242/jcs.063016
43. Rüter C, Hardwidge PR (2014) 'Drugs from bugs': bacterial effector proteins as promising biological (immune-) therapeutics. FEMS Microbiol Lett 351:126–132. https://doi.org/10.1111/1574-6968.12333
44. Rüter C, Schmidt MA (2017) Cell-penetrating bacterial effector proteins: better tools than targets. Trends Biotechnol 35:109–120
45. Scharnert J, Greune L, Zeuschner D, Lubos ML, Alexander Schmidt M, Rüter C (2013) Autonomous translocation and intracellular trafficking of the cell-penetrating and immune-suppressive effector protein YopM. Cell Mol Life Sci 70:4809–4823. https://doi.org/10.1007/s00018-013-1413-2
46. Scheibner F, Marillonnet S, Büttner D (2017) The TAL effector AvrBs3 from *Xanthomonas campestris* pv. *vesicatoria* contains multiple export signals and can enter plant cells in the absence of the type III secretion translocon. Front Microbiol 8:2180
47. Seyedarabi A, Sullivan JA, Sasakawa C, Pickersgill RW (2010) A disulfide driven domain swap switches off the activity of *Shigella* IpaH9.8 E3 ligase. FEBS Lett 584:4163–4168. https://doi.org/10.1016/j.febslet.2010.09.006
48. Stewart KM, Horton KL, Kelley SO (2008) Cell-penetrating peptides as delivery vehicles for biology and medicine. Org Biomol Chem 6:2242–2255. https://doi.org/10.1039/b719950c
49. Stolle AS, Norkowski S, Körner B, Schmitz J, Lüken L, Frankenberg M, Rüter C, Schmidt MA (2017) T3SS-independent uptake of the short-trip toxin-related recombinant NleC effector of enteropathogenic *Escherichia coli* leads to NF-kappaB p65 cleavage. Front Cell Infect Microbiol 7:119. https://doi.org/10.3389/fcimb.2017.00119
50. Suzuki S, Mimuro H, Kim M, Ogawa M, Ashida H, Toyotome T, Franchi L, Suzuki M, Sanada T, Suzuki T, Tsutsui H, Nunez G, Sasakawa C (2014) *Shigella* IpaH7.8 E3 ubiquitin ligase targets glomulin and activates inflammasomes to demolish macrophages. Proc Natl Acad Sci USA 111:E4254–E4263. https://doi.org/10.1073/pnas.1324021111
51. Thorén PE, Persson D, Isakson P, Goksör M, Önfelt A, Nordén B (2003) Uptake of analogs of penetratin, Tat(48-60) and oligoarginine in live cells. Biochem Biophys Res Commun 307:100–107
52. Toyotome T, Suzuki T, Kuwae A, Nonaka T, Fukuda H, Imajoh-Ohmi S, Toyofuku T, Hori M, Sasakawa C (2001) *Shigella* protein IpaH(9.8) is secreted from bacteria within mammalian cells and transported to the nucleus. J Biol Chem 276:32071–32079. https://doi.org/10.1074/jbc.m101882200
53. van den Ent F, Lowe J (2006) RF cloning: a restriction-free method for inserting target genes into plasmids. J Biochem Biophys Methods 67:67–74
54. Varkouhi AK, Scholte M, Storm G, Haisma HJ (2011) Endosomal escape pathways for delivery of biologicals. J Control Release 151:220–228. https://doi.org/10.1016/j.jconrel.2010.11.004
55. Wang F, Jiang Z, Li Y, He X, Zhao J, Yang X, Zhu L, Yin Z, Li X, Wang X, Liu W, Shang W, Yang Z, Wang S, Zhen Q, Zhang Z, Yu Y, Zhong H, Ye Q, Huang L, Yuan J (2013) *Shigella flexneri* T3SS effector IpaH4.5 modulates the host inflammatory response via interaction with NF-kappaB p65 protein. Cell Microbiol 15:474–485. https://doi.org/10.1111/cmi.12052
56. Waterhouse AM, Procter JB, Martin DM, Clamp M, Barton GJ (2009) Jalview Version 2—a multiple sequence alignment editor and analysis workbench. Bioinformatics 25:1189–1191. https://doi.org/10.1093/bioinformatics/btp033
57. Wei C, Wang Y, Du Z, Guan K, Cao Y, Yang H, Zhou P, Wu F, Chen J, Wang P, Zheng Z, Zhang P, Zhang Y, Ma S, Yang R, Zhong H, He X (2016) The *Yersinia* type III secretion effector YopM is an E3 ubiquitin ligase that induced necrotic cell death by targeting NLRP3. Cell Death Dis 7:e2519. https://doi.org/10.1038/cddis.2016.413
58. Yadav M, Zhang J, Fischer H, Huang W, Lutay N, Cirl C, Lum J, Miethke T, Svanborg C (2010) Inhibition of TIR domain signaling by TcpC: MyD88-dependent and independent effects on *Escherichia coli* virulence. PLoS Pathog 6:e1001120. https://doi.org/10.1371/journal.ppat.1001120
59. Young BM, Young GM (2002) YplA is exported by the Ysc, Ysa, and flagellar type III secretion systems of *Yersinia enterocolitica*. J Bacteriol 184:1324–1334
60. Zheng Z, Wei C, Guan K, Yuan Y, Zhang Y, Ma S, Cao Y, Wang F, Zhong H, He X (2016) Bacterial E3 ubiquitin ligase IpaH4.5 of *Shigella flexneri* targets TBK1 to dampen the host antibacterial response. J Immunol 196:1199–1208. https://doi.org/10.4049/jimmunol.1501045
61. Zhu Y, Li H, Hu L, Wang J, Zhou Y, Pang Z, Liu L, Shao F (2008) Structure of a *Shigella* effector reveals a new class of ubiquitin ligases. Nat Struct Mol Biol 15:1302–1308